Reaction of Methane with $Rh(PH_3)_2Cl$: A Dynamical Density Functional Study

Peter Margl,† Tom Ziegler,*,† and Peter E. Blöchl‡

Contribution from the Department of Chemistry, University of Calgary, 2500 University Drive N.W., T2N 1N4 Calgary, Alberta, Canada, and IBM Research Division, Zurich Research Laboratory, CH-8803 Rüschlikon, Switzerland

Received August 11, 1995⊗

Abstract: Some of the key steps in the alkane carbonylation processes developed by Sakakura and Tanaka have been modeled by density functional theory. The catalytic carbonylation cycle involves photochemical activation of the precursor compound $Rh(PR_3)_2Cl(CO)$ (**1**), resulting in the 14-electron species $Rh(PR_3)_2Cl$ (**2**), which activates the C−H bond of hydrocarbons. The model precursor compound $Rh(PH_3)_2Cl(CO)$ has a ground state structure with the phosphine ligands in a trans position, whereas **2** for R = H prefers a cis arrangement of the phosphines (*cis*-**2a**) and has a closed shell singlet ground state. The model species **2** with R = H adds a C−H methane bond to produce $Rh(PH_3)_2Cl(H)(CH_3)$ (**5**), after the formation of the η^2-methane complex $Rh(PH_3)_2Cl(\eta^2\text{-}CH_4)$ (**3**). The trans conformation *trans*-**2a** of $Rh(PH_3)_2Cl$ is more reactive toward the C−H methane bond than *cis*-**2a** and forms a stronger η^2-methane complex. The activation product $Rh(PH_3)_2Cl(H)(CH_3)$ (**5**) reacts with another CO to form $Rh(PH_3)_2Cl(H)(CH_3)(CO)$ (**6**), which can either eliminate methane to form **1** or undergo further transformation to eventually form acetaldehyde and **1**. The elimination of methane is relatively facile with kinetic barriers of 72 kJ/mol (trans) and 57 kJ/mol (cis), respectively. In addition, the elimination reactions are exothermic by respectively 112 kJ/mol (trans) and 125 kJ/mol (cis). It is thus clear that alkane elimination seriously can impede the carbonylation cycle. The catalytic activity can also be reduced by dimerization of $Rh(PH_3)_2Cl$. The present investigation combines "static" calculations of the stationary points on the potential surface with first principles molecular dynamics calculations based on the Car−Parrinello−Projector−Augmented−Wave method.

1. Introduction

Functionalization of hydrocarbons through activation of the chemically rather inert C−H bond is one of the more challenging problems in organometallic chemistry. Since the pioneering work of Bergman,[1a] Graham,[1b] and Jones,[1c] several groups have discovered new transition metal species capable of activating alkane C−H bonds at or below room temperature. Experiments[1,2] as well as theoretical calculations[3] support the view that iridium- and rhodium-based systems are among the best suited for activation of a C−H bond.

The early work on C−H activation[1,2] was concerned with the basic reaction in which a C−H bond is broken. However, later on Sakakura[4] and Tanaka developed complete catalytic cycles for C−H bond functionalizations involving carbonylation, isonitrile insertion, C=C double bond insertion etc. The functionalizations are all based on rhodium catalysts activated by photolysis. The complete cycle for the carbonyl insertion reaction is shown in Figure 1.

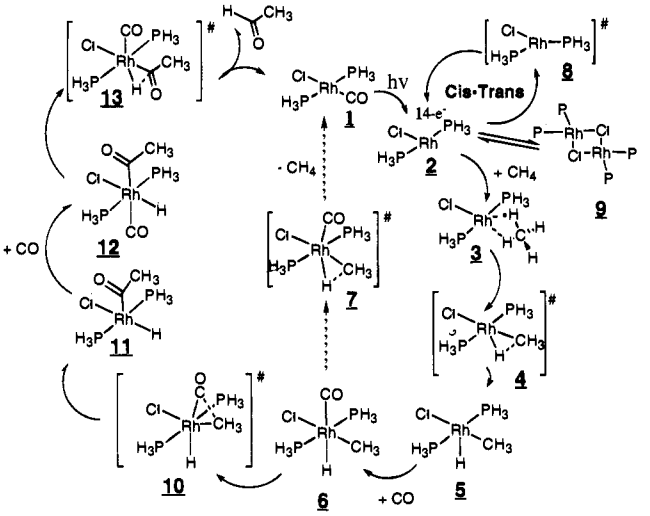

Figure 1. Catalytic cycle for the carbonylation of methane with $Rh(PH_3)_2Cl$. The stages of the reaction are indicated with numbers (**1**−**13**).

The C−H activation steps **2** → **3** → **4** of Figure 1 have already been investigated in a theoretical study by Koga and Morokuma[3c] and by Blomberg et al.[3f] However, a full theoretical analysis of a complete C−H functionalization cycle has not yet been provided. We intend to carry out such an analysis for the carbonyl insertion reaction shown in Figure 1 by using static and dynamic methods based on density functional theory[5] (DFT). In the present investigation we study the possible reaction pathways for the oxidative addition, **2** → **3** → **4** → **5**,

† University of Calgary.
‡ IBM Research Division.
⊗ Abstract published in *Advance ACS Abstracts*, December 1, 1995.

(1) (a) Janowicz, A. H.; Bergman, R. G. *J. Am. Chem. Soc.* **1982**, *104*, 352. (b) Hoyano, J. K.; Graham, W. A. G. *J. Am. Chem. Soc.* **1982**, *104*, 3724. (c) Jones, W. D.; Feher, F. J. *J. Am. Chem. Soc.* **1982**, *104*, 4240.
(2) (a) Crabtree, R. H. *Chem. Rev.* **1985**, *85*, 245. (b) Jones, W. D.; Feher, F. J. *Acc. Chem. Res.* **1989**, *22*, 91.
(3) (a) Low, J. J.; Goddard, W. A., III. *J. Am. Chem. Soc.* **1984**, *106*, 8321. (b) Ziegler, T.; Tschinke, V.; Fan, L.; Becke, A. D. *J. Am. Chem. Soc.* **1989**, *111*, 9177. (c) Koga, N.; Morokuma, K. *J. Phys. Chem.* **1990**, *94*, 5454. (d) Song, J.; Hall, M. B. *Organometallics* **1993**, *12*, 3118. (e) Siegbahn, P. E. M.; Svensson, M. *J. Am. Chem. Soc.* **1994**, *116*, 10124. (f) Blomberg, M. R. A.; Siegbahn, P. E. M.; Svensson, M. *J. Am. Chem. Soc.* **1992**, *114*, 6095.
(4) (a) Sakakura, T.; Tanaka, M. *Chem. Phys. Lett.* **1987**, *249*, 1113. (b) Tanaka, M.; Sakakura, T. In *Advances in Chemistry Series*, Vol. 230; Moser, W. R., Slocum, D. W., Eds.; American Chemical Society: Washington, DC, 1992; p 181. (c) Sakakura, T.; Sodeyama, T.; Sasaki, K.; Wada, K.; Tanaka, M. *J. Am. Chem. Soc.* **1990**, *112*, 7221.

0002-7863/95/1517-12625$09.00/0

and reductive elimination, **6** → **7** → **1**, of methane. Especially, we hope to elucidate the hitherto inaccessible dynamical features of these reactions using the powers of the Car–Parrinello[6] (CP) method. The remaining part of the cycle involving species **10**–**13** will be reported in connection with a subsequent study.[7]

Elementary reaction steps in homogeneous catalysis have been investigated with increasing success by conventional electronic structure methods over the past decade.[8] Studies of this kind can provide minimum energy paths on the potential energy surface connecting reactant(s), transition state(s), and product(s). The conventional electronic structure methods afford essentially a static view of chemical reactions, although dynamical aspects and temperature effects can be included by statistical methods after mapping out the potential energy surfaces near the minimum energy paths. However, such a mapping is costly in terms of man hours and computer resources.

Car and Parrinello (CP) have proposed a DFT-based scheme in which the dynamics of a system can be studied from first principles without recourse to precalculated and fitted potential surfaces. Unfortunately, it is only practical to explore the regions of phase space relevant for chemical reactions with straightforward dynamics if low barriers are involved. For processes with high or even moderate barriers (>30 kJ/mol), the events of interest occur sparsely, if at all. Most of the simulation time is thus spent in the more trivial places in phase space, rendering the simulation computationally costly and inefficient.

We combine in the present study conventional electronic structure calculations with the CP method. This is accomplished by employing a technique based on constrained CP dynamics, where we introduce fictitious dynamics along a chosen reaction coordinate in order to sample the phase space in the vicinity of the transition state. The appropriate reaction coordinate as well as the area around the transition state is determined by conventional electronic structure calculations based on the Amsterdam Density Functional program system[9] (ADF) whereas the CP dynamics is carried out with the projector augmented wave method (PAW) due to Blöchl.[10]

2. Computational Details

Stationary points on the potential energy surface were calculated with the program ADF, developed by Baerends[11] et al. and vectorized by Ravenek.[12] The numerical integration scheme applied for the calculations was developed by te Velde[13] et al. The geometry optimization procedure was based on the method due to Versluis[14] and Ziegler. The electronic configurations of the molecular systems were described by a triple-ζ basis set on rhodium[15] for 4s, 4p, 4d, 5s, and 5p. Double-ζ STO basis sets were used for carbon (2s, 2p), hydrogen (1s), phosphorus (3s, 3p), chlorine (3s, 3p), and oxygen (2s, 2p), augmented with a single 3d polarization function except for hydrogen where a 2p function was used. The $1s^2 2s^2 2p^6 3s^2 3d^{10}$ configuration on rhodium, the $1s^2$ shell on carbon and oxygen, and the $1s^2 2s^2 2p^6$ shells on phosphorus and chlorine were assigned to the core and treated within the frozen core approximation.[11] A set of auxiliary[16] s, p, d, f, and g STO functions, centered on all nuclei, was used in order to fit the molecular density and present Coulomb and exchange potentials accurately in each SCF cycle. Energy differences were calculated by including the local exchange-correlation potential by Vosko[17] et al. with Becke's[18] nonlocal exchange corrections and Perdew's[19] nonlocal correlation correction. Geometries were optimized including nonlocal corrections. First-order scalar relativistic corrections[20] were added to the total energy, since a perturbative relativistic approach is sufficient for 4d metals. Symmetry constraints were used wherever consistent with the physical circumstances to accelerate calculations. Saddle point determinations were initialized by a linear transit search from reactant to product along an assumed reaction coordinate. In each step along the reaction coordinate all other degrees of freedom were optimized. The structure representing the energy maximum was used as the initial guess in a subsequent full optimization of the transition state.

All reported molecular dynamics simulations were carried out with the Car–Parrinello projector augmented wave (CP-PAW) code developed by Blöchl.[10] The wave function is expanded in plane waves up to an energy cutoff of 30 Ry. The frozen-core approximation was applied for shells including and below the 3d electrons of Rh, the 2p electrons of Cl and P, and the 1s electrons of O and C. Core data were imported from scalar relativistic atomic calculations. We use periodic boundary conditions with a 11.3 Å fcc cell. All simulations were performed using the local density approximation in the parametrization of Perdew and Zunger,[21] with gradient corrections due to Becke[18] and Perdew.[19] Long-range electrostatic interactions between different cells are eliminated using a method developed by Blöchl.[22] A time step of 10 au is used, correcting the mass of the nuclei to account for the drag of the electrons[23] in the coupled dynamics integrated with the Verlet[24] algorithm. The temperature of the nuclei is controlled by a Nosé[25] thermostat, which creates a canonical (NVT) ensemble. To sample phase space in the vicinity of the transition state, we choose a reaction coordinate (RC) which is kept constrained during the dynamics using SHAKE[26] constraints. It is desirable that the RC has a high projection onto the IRC[27] (intrinsic reaction coordinate). All other degrees of freedom are allowed to evolve naturally in time. By slowly varying the constraint, phase space in the vicinity of the transition state can be sampled dynamically,[28,29] leading to undisturbed dynamics for all motions which are orthogonal to the RC and to fictitious dynamics along the RC. This allows to investigate even high-lying transition states, such as those encountered in the present study. The speed of the RC scan was determined by a third-power polynomial, to avoid sudden accelerations which disrupt the coupled electron-ion dynamics.

Time-dependent vibrational frequencies were calculated from 0.4 ps windows of the atomic velocities, using either the Fourier transform[30a] or the MUSIC spectral estimation technique.[30b] Due to this short sampling interval, we give vibrational frequencies only within an accuracy of 50 cm^{-1}. To achieve an evenly distributed thermal

(5) (a) Parr, R. G.; Yang, W. *Density Functional Theory of Atoms and Molecules*; Oxford University Press: New York, 1989. (b) Ziegler, T. *Chem. Rev.* **1991**, *91*, 651.
(6) Car, R.; Parrinello, M. *Phys. Rev. Lett.* **1985**, *55*, 2471.
(7) Margl, P.; Ziegler, T.; Blöchl, P., work in progress.
(8) (a) *Theoretical Aspects of Homogeneous Catalysts*; van Leeuwen, P. W. N. M., Morokuma, K., van Lenthe, J. H., Eds.; Kluwer Academic Publishers: Dordrecht, The Netherlands, 1995. (b) Koga, N.; Morokuma, K. *Chem. Rev.* **1991**, *91*, 823.
(9) ADF version 1.1.3.
(10) Blöchl, P. E. *Phys. Rev. B* **1994**, *50*, 17953.
(11) (a) Baerends, E. J.; Ellis, D. E.; Ros, P. *Chem. Phys.* **1973**, *2*, 41. (b) Baerends, E. J. Ph.D. Thesis, Vrije Universiteit, Amsterdam, 1975.
(12) Ravenek, W. In *Algorithms and Applications on Vector and Parallel Computers*; te Riele, H. J. J., Dekker, Th. J., van de Horst, H. A., Eds.; Elsevier: Amsterdam, 1987.
(13) (a) Boerrigter, P. M.; te Velde, G.; Baerends, E. J. *Int. J. Quantum Chem.* **1988**, *33*, 87. (b) te Velde, G.; Baerends, E. J. *J. Comput. Phys.* **1992**, *99*, 84.
(14) Versluis, L.; Ziegler, T. *J. Chem. Phys.* **1988**, *88*, 322.
(15) (a) Snijders, G. J.; Baerends, E. J.; Vernooijs, P. *At. Nucl. Data Tables* **1982**, *26*, 483. (b) Vernooijs, P.; Snijders, G. J.; Baerends, E. J. Slater Type Basis Functions for the whole Periodic System. Internal Report, Free University of Amsterdam, The Netherlands, 1981.
(16) Krijn, J.; Baerends, E. J. Fit functions in the HFS method. Internal Report (in Dutch), Free University of Amsterdam, The Netherlands, 1984.
(17) Vosko, S. H.; Wilk, L.; Nusair, M. *Can. J. Phys.* **1990**, *58*, 1200.
(18) Becke, A. D. *Phys. Rev. A* **1988**, *38*, 3098.
(19) Perdew, J. P. *Phys. Rev. B* **1986**, *33*, 8822; **1986**, *34*, 7406.
(20) (a) Snijders, J. G.; Baerends, E. J. *Mol. Phys.* **1978**, *36*, 1789. (b) Snijders, J. G.; Baerends, E. J.; Ros, P. *Mol. Phys.* **1979**, *38*, 1909. (c) Ziegler, T.; Tschinke, V.; Baerends, E. J.; Snijders, J. G.; Ravenek, W. *J. Phys. Chem.* **1989**, *93*, 3050.
(21) Perdew, J. P.; Zunger, A. *Phys. Rev. B* **1981**, *23*, 5048.
(22) Blöchl, P. E. *J. Chem. Phys.* **1995**, *103*, 7422.
(23) Blöchl, P. E.; Parrinello, M. *Phys. Rev. B* **1992**, *45*, 9413.
(24) Verlet, L. *Phys. Rev.* **1967**, *159*, 98.
(25) (a) Nosé, S. *Mol. Phys.* **1984**, *52*, 255. (b) Hoover, W. G. *Phys. Rev. A* **1985**, *31*, 1695.
(26) Ryckaert, J.-P.; Ciccotti, G.; Berendsen, H. J. *J. Comput. Phys.* **1977**, *23*, 327.
(27) Fukui, K. *Acc. Chem. Res.* **1981**, *14*, 363.

Chart 1

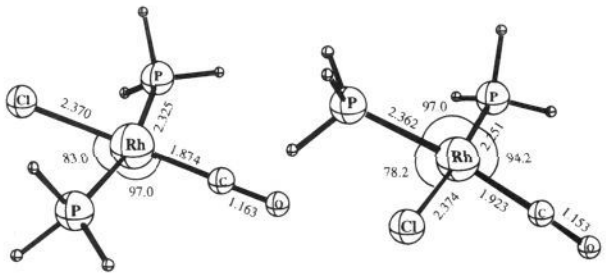

excitation, the dynamics were initialized with vibrational eigenvectors taken from ADF calculations and the nuclei were slowly heated with a sinusoidal pulse to avoid detachment of the electrons from the Born–Oppenheimer surface by abrupt changes in the nuclear velocities.

3. The Calculation of Stationary Points

We shall in this section discuss structures and relative energies of stationary points on the possible reaction pathways for the oxidative addition, **2** → **3** → **4** → **5**, and reductive elimination, **6** → **7** → **1**, of methane, Figure 1. Methane was taken as a model for alkanes actually functionalized by C–H activation in the studies due to Sakakura[4] and Tanaka. For all calculations PMe_3 was modeled by PH_3. Throughout this paper, we refer to different stages on the reaction coordinate with numbers (**1**–**13**), additionally specifying the substitution pattern of the PH_3 groups (cis/trans). If more than one isomer can occur at one stage, the distinction is made with alphanumerics (a–f).

The 16-Electron Precursor Complex $Rh(PH_3)_2ClCO$ (1). The starting point for the carbonylation cycle of Figure 1 is the square planar Vaska-type complex **1**. Sakakura[4] and Tanaka did not report on the conformation of the precursor complex **1**. A geometry optimization yields that the trans isomer, *trans*-**1** of Chart 1, is 37 kJ/mol more stable than the cis isomer *cis*-**1** of Chart 1. The electronic preference for *trans*-**1** can be explained by the relative strength of CO, PR_3, and Cl^- as trans-destabilizing ligands[31] with CO > PR_3 ≫ Cl^-. The *trans*-**1** conformation should also be favored on steric grounds for more bulky phosphines. It was assumed that the electronic ground state of **1** is a closed-shell singlet since both isomers have HOMO–LUMO splittings of >2.5 eV.

The actual catalyst in Figure 1 is the 14-electron tricoordinated species $Rh(PH_3)_2Cl$ (**2**). It is generated from **1** by photoejection of a CO ligand[4,32] with light of wavelengths between 295 and 365 nm. It follows from the orbital level diagram of *trans*-**1** given in Figure 2 that this molecule absorbs light with wavelengths between 295 and 365 nm in connection with metal-to-ligand charge-transfer (MLCT) excitations. The electron transfer takes place from the metal-based $d_{x^2-y^2}$ HOMO to HOMO+2 (3.0 eV above HOMO) or HOMO+3 (3.8 eV above HOMO). The two higher lying orbitals HOMO+2 and HOMO+3 are π^*_{CO} on the basis of out of phase contributions from the d_{zy} and d_{zx} metal orbitals, respectively. It is thus understandable that the MLCT excitations can give rise to CO elimination. We note that the orbitals HOMO+2 and HOMO+3 are also antibonding with respect to the Rh–Cl interaction. However, due to the much larger Rh–Cl bond energy, Rh–Cl dissociation would not be a facile process.

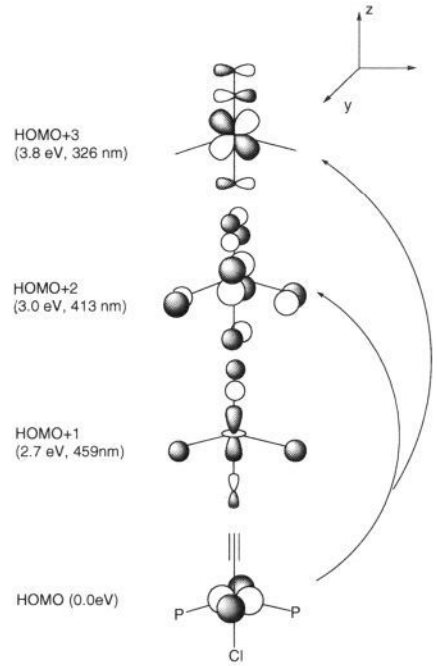

Figure 2. Schematic view of the orbitals in *trans*-**1** relevant for photodissociation.

The 14-Electron Species $Rh(PH_3)_2Cl$ (2). The preferred conformation for the 14-electron tricoordinated catalyst $Rh(PH_3)_2Cl$ (**2**) is *cis*, *cis*-**2a** of Chart 2. The corresponding trans structure, *trans*-**2a** of Chart 2, is 69 kJ/mol higher in energy. The electronic preference for a cis conformation can again be explained by the relative strength of PR_3 and Cl^- as trans-destabilizing[31] ligands with PR_3 > Cl^-.

Since the splitting between the HOMO and the LUMO (Figure 3) in **2** is quite small, geometry optimizations were carried out for the closed-shell singlet $(a_2)^2(b_1)^2(b_2)^2(1a_1)^2(2a_1)^0$ $^1A_1$, *cis*-**2a** and *trans*-**2a** of Chart 2, triplet $^3A_1$ $(a_2)^2(b_1)^2(b_2)^2$-$(1a_1)^1(2a_1)^1$, *cis*-**2b** and *trans*-**2b** of Chart 2, and open-shell singlet $^1A_1$ $(a_2)^2(b_1)^2(b_2)^2(1a_1)^1(2a_1)^1$ for both isomers. It turns out that the closed-shell singlet state is of lowest energy for both isomers, *cis*-**2a** and *trans*-**2a**, followed by the triplet, *cis*-**2b** and *trans*-**2b**, and the open-shell singlet states, see Figure 4. For the more stable cis conformation, the triplet and the open-shell singlet are respectively 84 and 103 kJ/mol above the closed-shell singlet. For the trans conformation, the triplet and the open-shell singlet are respectively 20 and 51 kJ/mol

(28) Integrating the force on the reaction coordinate (RC) is a possible way to determine the free energy ΔF of the reaction as

$$\Delta F = \int_0^1 \langle \partial E/\partial\lambda \rangle|_{\lambda,T}\, d\lambda$$

where λ is just the reaction coordinate running between 0 (begin of the reaction) and 1 (end of the reaction) and the integrand is the appropriately scaled averaged force on the reaction coordinate sampled at constant temperature and λ. However, application of the "slow growth technique" to determine ΔF requires a hysteresis curve to be sampled which accounts for the effects of finite RC scan velocity. Successful application would also require a method to deal with the abrupt releases of kinetic energy into specific channels which occur when a chemical reaction takes place, since these can lead to deviations from thermal equilibrium. Additionally, preliminary tests have shown that, in order to obtain accurate values for ΔF, the simulation time (currently ≈ 5 ps) must probably be increased by an order of magnitude.

(29) Straatsma, T. P.; Berendsen, H. J. C.; Postma, J. P. M. *J. Chem. Phys.* **1986**, *85*, 6720.

(30) (a) Allen, M. P.; Tildesley, D. J. *Computer Simulation of Liquids*; Clarendon Press: Oxford, 1987. (b) Schmidt, R. O. *IEEE Trans. Antennas Propag.* **1989**, AP 34, 276.

(31) Atwood, J. D. In *Inorganic and Organometallic Reaction Mechanisms*; Brooks/Cole Publishing Co.: Monterey, 1985.

(32) Ford, P. C.; Belt, S. T. In *Advances in Chemistry Series*, Vol. 230; Moser, W. R., Slocum, D. W., Eds.; American Chemical Society: Washington, DC, 1992; p 105.

Chart 2

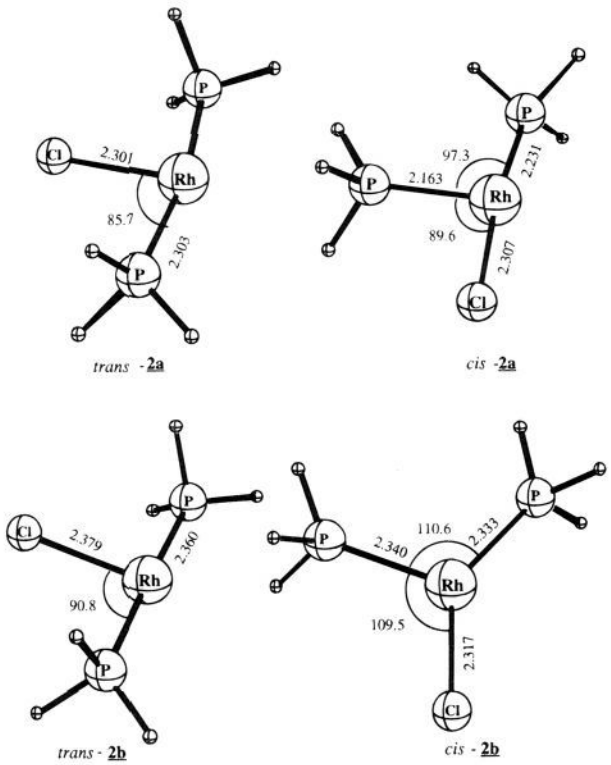

above the closed-shell singlet. Thus, the three states are closer together in the less favorable trans conformation, Figure 4.

The Cl−Rh−P angles for the triplet and open-shell singlet states of the trans conformation are larger (91° and 92°) than for the singlet ground state (86°). The same holds for the cis conformation, in which this effect is even more pronounced. Thus, the Cl−Rh−$P_{(cis)}$ angle is 90° for the closed-shell singlet, *cis*-**2a**, whereas it is 110° for the open-shell singlet and the triplet, *cis*-**2b**. The larger Cl−Rh−P angle results in a reduction of the antibonding metal−ligand interaction of the $2a_1$ orbital, Figure 3, which is occupied in the open-shell singlet and triplet states.

The two singlet isomers for the tricoordinated model catalyst $Rh(PH_3)_2Cl$ (**2**) (+ free CO) lie respectively 278 kJ/mol, *trans*-**2a**, and 172 kJ/mol, *cis*-**2a**, above the 16-electron precursor complexes $Rh(PH_3)_2(CO)Cl$ *trans*-**1a** and *cis*-**1a**, which is in line with an experimental result[33] of 202 kJ/mol for the CO addition enthalpy of $Rh(P^iPr_3)_2Cl$.

It is most likely that the photoejection of CO from the ground state trans conformation of $Rh(PR_3)_2(CO)Cl$ in the first place will produce the trans conformation of $Rh(PR_3)_2Cl$. The cis conformation can then be produced by a subsequent isomerization. The rearrangement from *trans*-**2a** to *cis*-**2a** was calculated to have a kinetic barrier of 41 kJ/mol and proceeds via the Y-shaped transition state **8** of Chart 3. Thus, the cis−trans isomerization seems to be a feasible process once the photoejection of CO from $Rh(PR_3)_2ClCO$ has taken place.

The catalyst $Rh(PR_3)_2Cl$ might satisfy its unsaturated coordination by dimerizing to the less active species $[Rh(PR_3)_2Cl]_2$. We calculate the dimerization reaction *cis*-**2a** → $^1/_2[Rh(PH_3)_2Cl]_2$ to be exothermic by 87 kJ per mol of monomer, which agrees with an experimental result for the lower limit of the dimerization enthalpy of $Rh(P^iPr_3)_2Cl$ of 74 kJ/mol.[33] This means that dimerization should be an important factor for

(33) Wang, K.; Rosini, G. P.; Nolan, S. P.; Goldman, A. S. *J. Am. Chem. Soc.* **1995**, *117*, 5082.

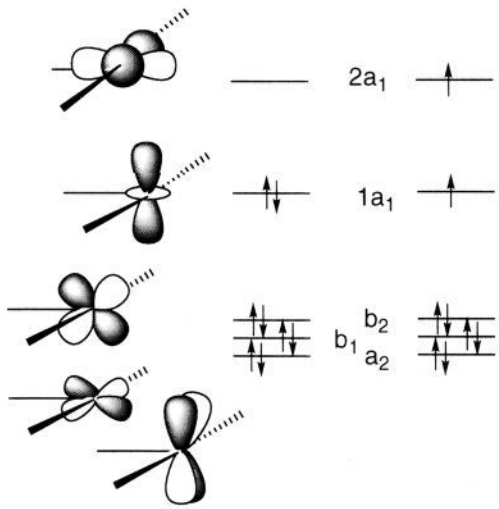

Figure 3. Schematic view of the metal orbitals in a ML_3 complex of C_{2v} symmetry.

determining the overall reaction rate once catalyst concentration is high enough to allow dimerization. Flash photolysis measurements of $RhCl(PPh_3)_2$ confirm this result.[34] The optimized structure for $[Rh(PR_3)_2Cl]_2$ (**9**) is shown in Chart 4.

Koga and Morokuma[3c] (KM) have also studied the 14-electron tricoordinated catalyst $Rh(PH_3)_2Cl$ (**2**). However, they only considered the trans conformer, which, according to our calculations, is the least stable isomer. KM optimized the trans structures for the triplet and two singlets on the Hartree−Fock level where electron correlation is neglected. The calculated Rh−Cl and Rh−P distances were rather long and exceeded those found here by 0.2 Å. On the basis of the HF structures, relative energies of the three states were evaluated by various post-HF methods in which electron correlation was taken into account. The three states in the trans conformation were in accordance with our calculations found to be close in energy. However, KM found the triplet state to be of lowest energy. A correlated ab initio study by Blomberg et al.[3f] on the relative stabilities of different electronic states of *trans*-**2** also found the triplet state to be lowest, but it was noted that the splitting between the singlet and triplet state is so small (13 kJ/mol) that a more accurate description of correlation might reverse the order of stability. Our calculations make use of correlated methods for energies as well as structures, and we conclude tentatively that $Rh(PH_3)_2Cl$ has a cis structure, *cis*-**2a**, with a closed-shell singlet ground state. It would be interesting to carry out correlated ab initio calculations on the structures and relative energies of both isomers for the three different states. We would also expect $Rh(PR_3)_2Cl$ with modest size phosphines such as PMe_3 to prefer a cis conformation. However, for more bulky phosphines the trans conformation of $Rh(PR_3)_2Cl$ might become more stable.

The η^2-Adduct $Rh(PH_3)_2Cl(\eta^2\text{-}CH_4)$ (3) and the C−H Activation Step. The activation of a C−H bond in the methane substrate by **2**, Figure 1, starts with the formation of a stable η^2-adduct, $Rh(PH_3)_2Cl(\eta^2\text{-}CH_4)$ (**3**). Since **3** possesses a fairly large HOMO−LUMO gap (>2 eV), only the singlet ground state was considered. *cis*-**3** of Chart 5 is stabilized over the educts by 27 kJ/mol, *trans*-**3** of Chart 5 by 58 kJ/mol. Koga and Morokuma,[3c] using restricted Møller−Plesset fourth-order perturbation theory (MP4-SDTQ), obtained a stabilization of 74 kJ/mol of the adduct *trans*-**3** over the educts. Blomberg et al.[3f] find *trans*-**3** stabilized by 50 kJ/mol. It is also interesting

(34) Wink, D. A.; Ford, P. C. *J. Am. Chem. Soc.* **1987**, *109*, 436.

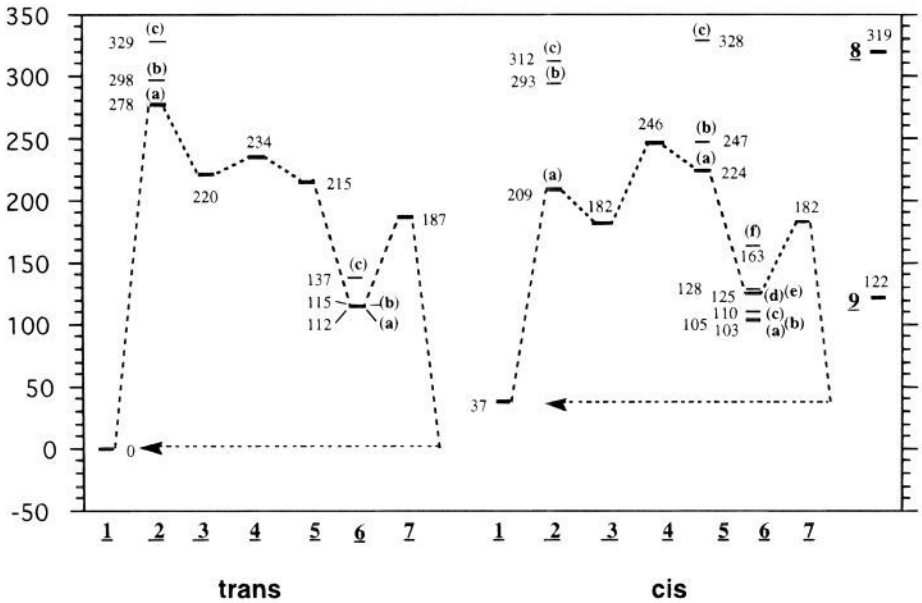

Figure 4. Energy profile for the methane activation, CO uptake, and subsequent elimination of methane. The *x* axis labels refer to different stages of the reaction, as in Figure 1. Different isomers or species occurring at a given stage are indicated by alphanumerics. Energy of free CO was added to **2**, **3**, **4**, **5**, **8**, and **9**. Energy of free CH_4 was added to **1**, **2**, **8**, and **9**. Energies are given in kJ/mol, relative to the species *trans*-**1** + CH_4. On the right-hand side of the graph the energies for the dimer and the transition state for cis−trans isomerization are given.

Chart 3

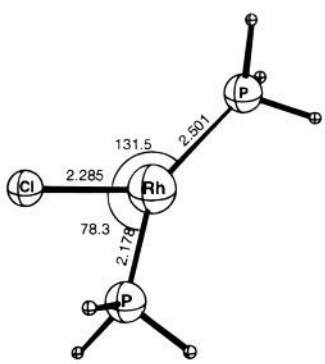

8

Chart 4

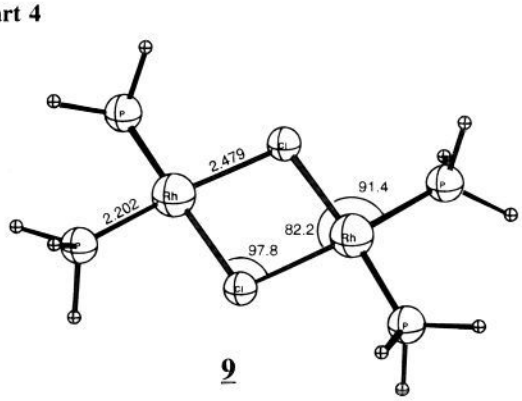

9

to note that the stabilization energy obtained by Song and Hall[35] for the agostic intermediate of the reaction of methane with CpRh(CO) of 61.9 kJ/mol is very similar to our value for the formation of *trans*-**3**.

trans-**3** has a Rh−C distance of 2.427 Å whereas the Rh−C distance of methane in *cis*-**3** is 2.562 Å. The agostic C−H bonds are elongated substantially from a ground state alkane

(35) Song, J.; Hall, M. B. *Organometallics* **1993**, *12*, 3118.

Chart 5

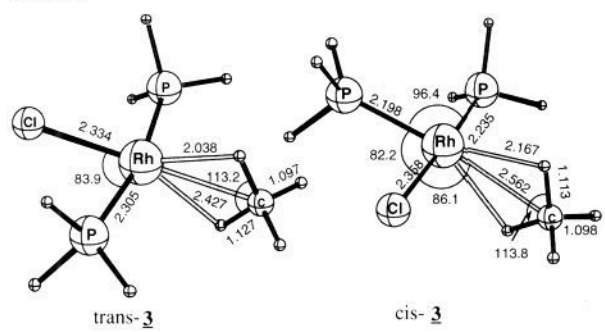

C−H distance of 1.098 to 1.127 Å in *trans*-**3** and 1.113 Å in *cis*-**3**. The longer Rh−C distance in *cis*-**3** correlates with a smaller value for the adduct formation energy. We attribute the weak adduct bond and long Rh−C distance in *cis*-**3** to the stronger trans-destabilizing effect of phosphine compared to chlorine. We note that the potential wells corresponding to out-of-plane motion of CH_4 as well as to rotation of methane about the axis parallel to the P−Rh−P axis are extremely shallow.

We have traced the path for the oxidative addition reaction with the linear transit method described in section 2, using the distance between the carbon and rhodium atoms as reaction coordinate. The structure representing the energy maximum on the approximate reaction path served subsequently as the starting point for a full transition state optimization.

The transition state for the oxidative addition reaction, **4** of Figure 1, occurs at C−H distances of 1.574 (trans) and 1.68 Å (cis), starting from *trans*-**3** and *cis*-**3**, respectively. Our C−H distance for *trans*-**4** of Chart 6 is comparable to the RHF estimate of 1.571 Å due to Koga and Morokuma. The same authors have also estimated a C−H distance of 1.35 Å for *trans*-**4** on the basis of MP2 calculations. However, this estimate is approximate and not based on a full geometry optimization at the MP2 level. Trans addition seems to occur

Chart 6

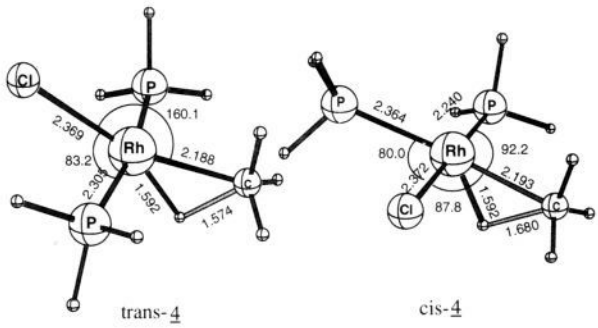

Chart 7

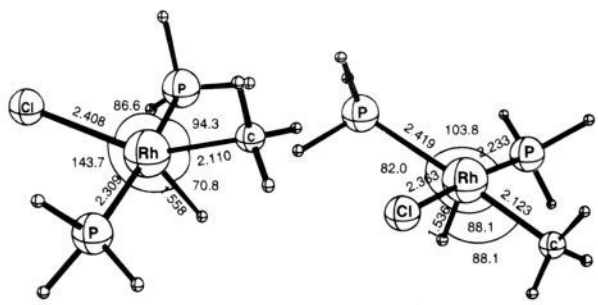

much "earlier" than cis addition, since the reaction **3** → **4** → **5** is exothermic by 5 kJ/mol in the trans case, Figure 4, whereas it is endothermic by 42 kJ/mol in the cis case. The cis barrier was calculated to be 64 kJ/mol compared to only 14 kJ/mol for the trans barrier. The higher barrier and unfavorable thermochemistry of the addition for *cis*-**3** compared to *trans*-**3** can be traced back to the stronger trans destabilization which is exerted by the phosphine ligand compared to chlorine for both the transition state **4** and the product **5**.

Koga and Morokuma[3c] found the transition state for C−H activation with *trans*-**2** to lie 14 kJ/mol above the η^2-complex and the exothermicity relative to the η^2-complex to be 31 kJ/mol at the MP4-SDTQ level. However, their energies are based on Hartree−Fock structures. At the HF level, the process is endothermic[3c] by 60 kJ/mol with a barrier of 80 kJ/mol. The study by Blomberg et al.[3f] arrived at a barrier height of 42 kJ/mol and an endothermicity relative to *trans*-**3** of 8.4 kJ/mol. Compared to our results, the potential surface of Koga and Morokuma is too attractive, whereas the one obtained by Blomberg et al. is too repulsive. The study by Song and Hall[35] gave a barrier of 17.2 kJ/mol for the activation of the methane C−H bond with CpRh(CO).

Since we found only a single transition state for each of the two pathways, the oxidative addition will always result in *trans*-**5a** or *cis*-**5a** of Chart 7. However, it is possible for 5-coordinated compounds such as **5** to undergo fluxional rearrangement processes, either of the Berry pseudorotation or the turnstile type. We therefore analyzed the relative stabilities of the different isomers of **5**. Of all the nine possible isomers (not taking into account stereoisomers), only four are found to be stationary, namely, *cis*-**5a**−**c** and *trans*-**5a** (Chart 8). All others relax into one of these four in the course of a geometry optimization.

All isomers of **5** exhibit a considerable deviation from the square pyramidal shape expected for a d^6 system. The deviations originate from the strong trans-destabilizing effect of both CH_3 and hydride. We conclude that *cis*-**3** electronically is the more stable of the two 14-electron tricoordinated catalysts

Chart 8

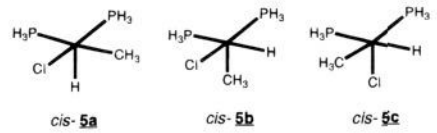

Chart 9

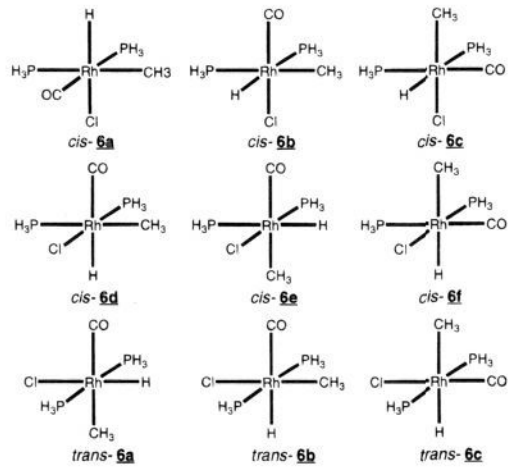

Chart 10

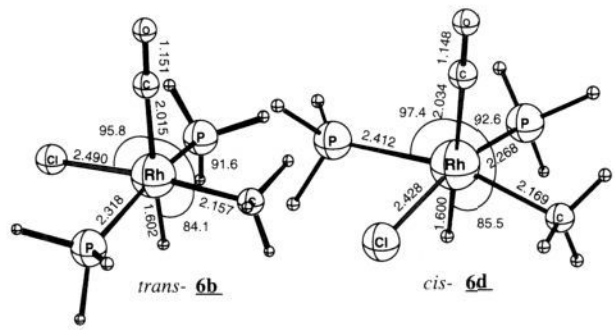

$Rh(PH_3)_2Cl$ generated by photoejection of CO from **1**. However, the energetically less stable trans conformer *trans*-**3** is more reactive toward the C−H alkane bond, so that the product of C−H activation will predominantly be *trans*-**5a**.

Carbon Monoxide Uptake by 5. The next step in the alkane carbonylation catalyzed by $Rh(PR_3)_2Cl$ is according to Figure 1 the addition of CO to the coordinatively unsaturated hydridoalkyl complex **5** formed from the addition of a C−H alkane bond to $Rh(PR_3)_2Cl$. This addition leads to the 6-coordinated saturated complex **6**, see Chart 9.

All isomers of **5** take up CO readily in a reaction which is exothermic by approximately 100 kJ/mol, Figure 4. Carbon monoxide uptake is a fast reaction, leaving only a small probability of fluxional rearrangement of **5** before it is blocked by coordination of CO. Therefore, the dominantly occurring isomers of **6** will be *cis*-**6d** and *trans*-**6b** of Chart 10, through the reactions *cis*-**5a** [*trans*-**5a**] + CO → *cis*-**6d** [*trans*-**6b**]. However, if the isomers *cis*-**5b** and *cis*-**5c** are populated, the reactions *cis*-**5b/c** + CO → *cis*-**6e/b** are also possible, though unlikely, since *cis*-**5b/c** lie 23 and 104 kJ/mol above *cis*-**5a**, respectively. We shall in the following focus our attention on two isomers, namely, *cis*-**6d** and *trans*-**6b** of Chart 10. Nevertheless, the energies of all isomers of **6** appear in Figure 4.

Elimination of Methane from the Carbonyl Complex 6. Sakakura[4] and Tanaka have suggested that the functionalization of alkanes by $Rh(PR_3)_2Cl$ might be retarded by the reductive

Chart 11

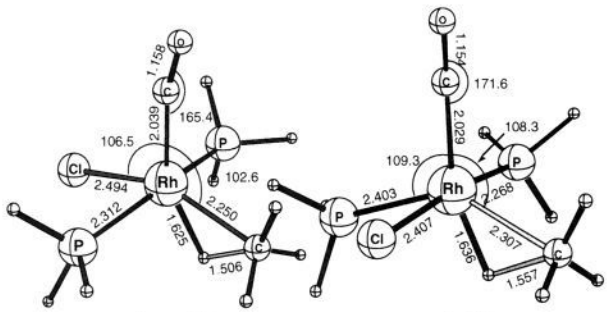

trans- **7b** *cis-* **7d**

elimination of alkanes from $H(R)Rh(PR_3)_2(CO)Cl$, thus regenerating the precatalyst $Rh(PR_3)_2(CO)Cl$ and R−H. This process is shown as **6** → **7** → **1** for the model cycle in Figure 1.

We have calculated the transition state **7** for the elimination reaction **6** → **1**. The procedure yields rather low-lying transition states, *trans*-**7b** and *cis*-**7d** of Chart 11, at C−H distances of 1.505 Å (trans) and 1.557 Å (cis), respectively. The kinetic barriers are 72 kJ/mol (trans) and 57 kJ/mol (cis), respectively. In addition, the elimination reactions are exothermic by respectively 112 kJ/mol (trans) and 125 kJ/mol (cis), Figure 4. Thus, the impeding reductive elimination reaction seems to be viable with a relatively modest activation barrier and a strong thermodynamic driving force. We shall in a subsequent study[7] investigate whether the productive steps **6** → **10** → **11** → **12** → **13** → **1** in the carbonylation of methane, Figure 1, can compete with the unproductive elimination sequence **6** → **1**.

4. CP-PAW Dynamical Calculations on the C−H Activation

The dynamics of the adduct formation process $Rh(PH_3)_2Cl$ (*trans*-**2**) + CH_4 → $Rh(PH_3)_2Cl(\eta^2\text{-}CH_4)$ (*trans*-**3**) as well as the addition of the C−H bond to the rhodium center, $Rh(PH_3)_2Cl(\eta^2\text{-}CH_4)$ (*trans*-**3**) → $CH_3(H)Rh(PH_3)_2Cl$ (*trans*-**5a**), was investigated with the CP-PAW method at 300 K. We initialize the dynamics at a point in phase space where the carbon atom of methane and the rhodium atom of *trans*-**2** are separated by 4.23 Å, slowly decreasing the C−Rh distance (henceforth referred to as the reaction coordinate, RC) over a period of 5.3 ps down to a RC length (RCL) of 2.01 Å. We refer to the RCL as the independent coordinate in Figure 5.

The contraction of the RC leads to a gradual increase of bonding between methane and rhodium, resulting in the formation of a loose η^1-adduct and subsequently, η^2-adduct **3**. Further contraction of the reaction coordinate weakens the C−H bonds, up to a point where the hydrogen atoms can jump from carbon to rhodium, which ultimately leads to the hydridomethyl product **5**. Structural and energetic characteristics of this process are shown in Figure 5.

The time dependence of the methane C−H bond lengths serves as an indicator of agostic interactions, which determine the bonding between the rhodium center and methane during the stages of the reaction before C−H activation occurs. Figure 5A displays the methane C−H bond lengths as a function of the RCL. The C−H stretching vibration has been filtered out for improved clarity. Between a RCL of 4.2 and 3.8 Å, the C−H bonds do not show significant deviations from the normal value of 1.1 Å. Below RCL = 3.8 Å, the C−H(2) distance represented by the dashed line increases, indicating that a weak η^1-interaction (H_3C−H(2)···Rh) is formed at this stage. The η^1-interaction is rather weak, which becomes apparent from the drops of the dashed line at RCL = 3.4 and 2.9 Å. These features correlate strongly with a large amplitude of the out-of-plane motion of CH_4 (Figure 5C). The η^1-agostic bond is therefore weakened when the CH_4 approaches from outside the molecular plane of *trans*-**2a**. At RCL = 2.6 Å, the η^2-species $Rh(PH_3)_2Cl(\eta^2\text{-}CH_4)$ (*trans*-**3**) is emerging, in agreement with our ADF result (section 3) which places the equilibrium Rh−C distance of *trans*-**3** at 2.427 Å. At the dynamic level, the two hydrogen atoms involved in the η^2-interaction (H(1) and H(2)) bind alternately to the rhodium atom, resulting in alternating changes in the corresponding C−H bond lengths (solid/dashed line, see inset in Figure 5A). This agrees well with the ADF finding that the potential well associated with this motion is extremely shallow.

At RCL = 2.2 Å (ADF, 2.118 Å) the transition state, *trans*-**4**, is reached, and the C−H(1) bond adds to the rhodium center leading to the product $CH_3(H)Rh(PH_3)_2Cl$, *trans*-**5a**. At this point the C−H(1) bond is broken abruptly (solid line, upper part Figure 5A) whereas the other hydrogen partner H(2) in the η^2-interaction regains a normal C−H distance of 1.1 Å (dashed line). The interval RCL = 2.2−2.0 Å corresponds to a stretching vibration of the Rh−C bond in the hydridomethyl product $CH_3(H)Rh(PH_3)Cl$ (*trans*-**5a**). In this stretching interval, the length of the broken C−H(1) bond varies strongly as the methyl carbon and the hydride attached to rhodium move along the H−Rh−C bending mode. This is stressed by the fact that the C−H(1) bond (solid) is almost restored at RCL = 2.1 Å, as indicated by a sharp dip of the solid line. Obviously, the H−Rh−C bending mode can serve as a possible reaction coordinate for reductive elimination of methane from *trans*-**5a**. The two other C−H bonds (H(3) dash-dotted, H(4) dotted in Figure 5A) do not interact appreciably with the metal center and therefore only oscillate weakly around 1.1 Å throughout the reaction. This is caused by the relatively early occurrence of the H_3C−H(2)···Rh bond at RCL = 3.8 Å, which fixes the orientation of the methane molecule relative to the metal center.

The bond distances between rhodium and the methane hydrogen atoms are depicted in Figure 5B as a function of RCL. At the beginning of the simulation, the methane molecule rotates freely (RCL = 4.2−4.0 Å), which can be seen in the rapidly oscillating Rh−H distances in this region. At RCL = 4.0 Å, a monohapto H_3C−H(2)···Rh interaction is formed (dashed line, see also Figure 5A), which weakly anchors the CH_4 molecule to *trans*-**2a**. At RCL = 2.6 Å, the η^2-interaction begins to form, so that there are two sets of lines, one oscillating around 3 Å (H(3) and H(4)) and one around 2 Å (H(1) and H(2)) Rh−H distance, with the strongest interaction flip-flopping between the two η^2-H atoms H(1) and H(2) (see inset). After the C−H activation has occurred (below 2.2 Å), the Rh−H(1) distance (solid line) drops to 1.5 Å, whereas the methyl hydrogens form a group above 2.5 Å. The unsuccessful reattachment of the hydride to the methyl group is indicated by a feature at 2.1 Å RCL. It becomes clear from these graphs that in solution the hydrocarbon will partake in extremely fast solvent exchange equilibria due to its high mobility and the reversibility of the agostic Rh−H bonding.

Figure 5C displays the Cl−Rh−CH_3 angle as a function of RCL. At the onset of the simulation, this angle measures the extent of out-of-plane motion by the CH_4 molecule, whereas in the final stages it serves to detect fluxional rearrangement about the rhodium center. At the beginning of the reaction, the methane molecule moves freely out of the $Rh(PH_3)_2Cl$ coordination plane, up to a Cl−Rh−CH_3 angle of 75°, which means that the probability of finding the methane molecule at this

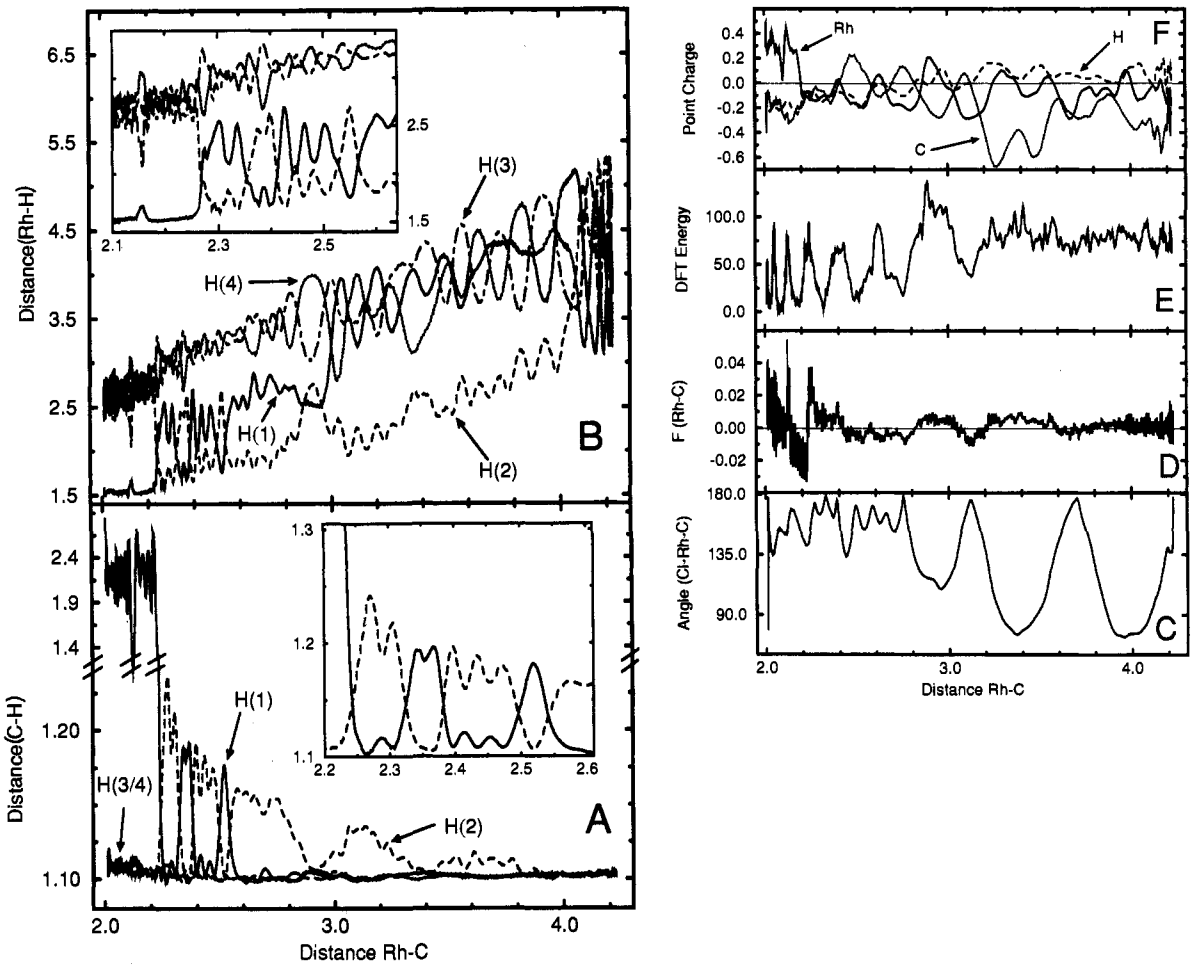

Figure 5. Geometric and energetic quantities as function of the reaction coordinate (RC = distance(Rh−C) during the reaction simulation of the C−H activation at 300 K. The reaction *trans*-**2a** + CH_4 → *trans*-**5a** proceeds from the right-hand side of the graph to the left. (A and B): each of the lines corresponds to a particular methane hydrogen atom, here labeled H(1)−H(4). Solid line represents H(1), dashed H(2), dash-dotted H(3), and dotted H(4). (A): Methane C−H distances. Upper part of graph is compressed to show large-amplitude C−H motion after C−H activation. (B) Distances between Rh and the methane hydrogens. Insets in (A) and (B) show the alternation in the bonding between Rh−H(1) and Rh−H(2) in the region of η^2-bonding. (C) Cl−Rh−C angle. (D) Force on the RC. (E) Total density functional energy, rescaled so that the lowest energy during the simulation equals zero. (F) Point charges on Rh (solid), H(1) (dashed), and C (dotted) calculated with the method described in ref 22. The scanning velocity was determined by a third-order polynomial to avoid abrupt accelerations. This results in a higher number of scan points per RCL unit near the beginning and the end of the simulation. The RC was scanned from 4.2 to 2.01 Å, which is below the Rh−C equilibrium distance. The horizontal thin lines at zero in (D) and (F) correspond to the zero of force and charge, respectively. All distances in angstrom units, angles in degrees, force in atomic units, energy in kJ/mol. For charges, −1 corresponds to the charge of one electron.

distance is almost spherical around the metal center in regions not excluded by the cone angles of the ligands. The methane passes through the molecular plane several times, at RCL = 3.7, 3.1, and 2.8 Å, before it becomes fixed close to the same plane, $\angle Cl-Rh-CH_3 \approx 180°$, by the onset of the η^2-interaction at RCL = 2.6 Å. On moving the reaction coordinate to values smaller than 2.1 Å, which is the equilibrium Rh−C distance in $CH_3(H)Rh(PH_3)_2Cl$ (*trans*-**5a**), we observe a high flexibility of the Cl−Rh−CH_3 angle. At this stage, the molecule undergoes rearrangement between the isomer *trans*-**5a** (Chart 7) and a square pyramidal arrangement (Cl−Rh−CH_3 90°; CH_3−Rh−H 90°; P−Rh−P 180°) where the methyl group occupies the apical position. The latter isomer is energetically very close to *trans*-**5a**; however it does not constitute a minimum point on the potential energy surface according to our ADF calculations (section 3). The interconversion reveals itself by the sharp dip at 2.0 Å, where the molecule rearranges once in this fashion and returns to *trans*-**5a**, which is in agreement with the ADF finding that *trans*-**5a** is the only stable trans isomer of **5**. However, this temporary rearrangement shows that the potential energy surface for fluxional processes around the metal center is rather flat. Also, this fluxional process is a direct consequence of the specific release of kinetic energy into the CH_3−Rh−H bending mode, following the dissociation of the C−H bond.

Figure 5D depicts the force on the reaction coordinate as a function of the RCL. A positive value means that the methane molecule wants to move away from rhodium, a negative value indicates that the reaction coordinate wants to contract. Between RCL = 4.2 and 3.8 Å, there is no appreciable deviation from zero, indicating a lack of strong Rh−C interactions. Below 3.6 Å, however, the force on the reaction coordinate begins to correlate with the Cl−Rh−C angle, becoming positive when the angle is small and negative when it is close to 180°. This means that only an approach path inside the plane of the complex is energetically favorable. Below RCL = 2.8 Å, when the dihapto interaction has been formed, the force becomes negative since the methane molecule is now pinned in the plane of the complex and the approach becomes favorable. Below 2.4 Å (equilibrium Rh−C distance for the η^2-complex *trans*-**3**), the system starts to approach the saddle point of the C−H activation and the force on the RC becomes positive again, corresponding to the energy needed to stretch the C−H bond. Once C−H activation has occurred (Figure 5A/B), the force rapidly drops to negative values, indicating that C−H activation

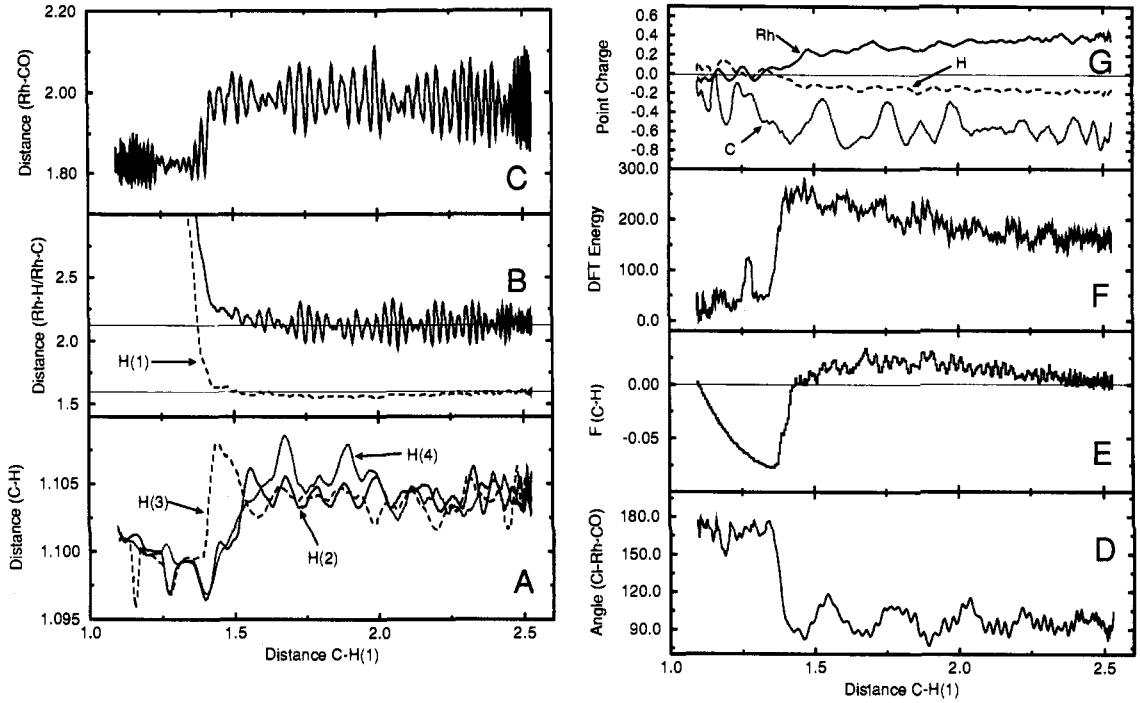

Figure 6. Geometric and energetic quantities as function of the reaction coordinate (RC = distance($C_{(methyl)}$–H(1)) during the reaction simulation of the reductive elimination at 300 K. The reaction *trans*-**6b** → *trans*-**1** + CH_4 proceeds from the right-hand side of the graph to the left. (A) C–H bond distances of the methyl group. Solid line C–H(2), dashed C–H(3), dotted C–H(4). (B) Rh–H(1) (dashed) and Rh–$C_{(methyl)}$ (solid) distance; thin lines indicate the respective equilibrium distances of *trans*-**6b**. (C) Rh–$C_{(carbonyl)}$ distance. (D) Cl–Rh–CO angle. (E) Force on the reaction coordinate, zero of force is indicated by horizontal thin line. (F) Total density functional energy, scaled as in Figure 5. (G) Charges on Rh (solid), H(1) (dashed), and $C_{(methyl)}$ (dotted). Units as in Figure 5.

is followed by contraction of the Rh–C bond. A sharp rise at 2.1 Å marks the temporary reattachment of the hydride to the methyl group. The force becomes zero shortly after 2.1 Å and rises to positive values as soon as the equilibrium Rh–C distance of *trans*-**5a** is crossed.

The density functional energy of the system as shown in Figure 5E correlates strongly with the Cl–Rh–C angle (Figure 5C), especially in the region below RCL = 3.5 Å, where bonding between CH_4 and Rh is already considerable. High energies correspond to a small angle, whereas low energies correspond to a favorable (in plane) approach angle of CH_4. Although curve E is rugged due to high thermal fluctuations, one can estimate that the overall reaction is exothermic by approximately 60 kJ/mol, in very good agreement with the ADF result of 63 kJ/mol. Also it is obvious that there is practically no barrier to C–H activation.

In Figure 5F, we use a method based on fitting an atom-centered Gaussian charge density[22] to the molecular electronic density in order to describe the shift of charge from the metal center to the ligand which occurs when oxidative addition takes place. The point charge values for carbon and the hydrogen atoms in free methane are respectively −0.33 and +0.083, and −0.1 for the Rh atom in free *trans*-**2a**. At the beginning of the reaction the lines start from their respective values in the free reactants. Below 3.0 Å RCL, at the onset of η^2-bonding, the charges coalesce around zero. A sharp increase of the solid line (Rh) at 2.2 Å RCL marks the dissociation of the C–H bond, indicating the charge transfer that is associated with the addition process. Correspondingly, the dashed (H) and dotted (C) lines drop due to the uptake of charge by the ligands. The intermediate reassociation of C and hydride occurring at 2.1 Å RCL is also marked by a sharp dip of the rhodium point charge, and the corresponding (but smaller) rise of the carbon charge.

Time-dependent vibrational analysis reveals that the methyl C–H stretch vibrations decrease by 100 cm^{-1} (from 3050 to 2950 cm^{-1}) after C–H activation, due to transfer of electron density from metal to antibonding ligand orbitals. At the same time, the Rh–Cl stretching frequency decreases by 50 cm^{-1} (from 350 to 300 cm^{-1}).

5. CP-PAW Dynamical Calculations on the CH_4 Elimination

The dynamics of the reductive elimination process $Rh(PH_3)_2Cl(H)(CH_3)(CO)$ (*trans*-**6b**) → $Rh(PH_3)_2Cl(CO)$ (*trans*-**1**) + CH_4 were investigated with the CP-PAW method at 300 K. We initialize the dynamics at the equilibrium geometry of *trans*-**6b**, where the carbon atom of the methyl group and the hydride atom of *trans*-**6b** are separated by 2.6 Å, slowly decreasing the C–H distance (RC) over a period of 4.84 ps down to a RCL of 1.098 Å, which is the equilibrium C–H distance of free methane. The RCL is the independent coordinate in Figure 6. Other choices of a RC are possible, such as the Rh–CH_3 distance. Our choice is justified since it provides the largest projection upon the true RC[36] up to the point of dissociation.

The contraction of the RC leads to dissociation of CH_4 from the metal center **6** and subsequent relaxation of the metal center to the equilibrium structure of **1**. Structural and energetic data of this process are depicted in Figure 6. Figure 6A displays the three C–H distances of the methyl group as a function of the RCL. High-frequency C–H vibrations have been filtered out as in Figure 5. Dissociation of CH_4 is indicated by a sharp dip in all three curves at a RCL of about 1.4 Å.[37] The contraction of the C–H bonds, which follows the reductive

(36) We note that it has the disadvantage that it makes the reaction irreversible so that CH_4 dissociation is forced by contraction of the RC, but subsequent association cannot be forced by expansion of the RC.

(37) The drops of the curves in Figure 6A at 1.3 and 1.2 Å are due to collisions of the released CH_4 molecule with periodic images (1.3 and 1.2 Å) of the metal complex and are therefore artifacts of our simulation technique. However, these collisions do not impair the quality of our results.

elimination, is related to the charge transfer from antibonding ligand orbitals to metal-based orbitals so that the C−H bonds are strengthened. Although the methyl group is rather mobile before CH_4 dissociation (Figure 6B), as expected no indication of agostic interactions between the methyl-bonded hydrogen atoms and rhodium is given by the C−H bond lengths.

CH_4 ejection is also clearly visible from a sharp rise of the curves in Figure 6B, which show the Rh−hydride (lower curve, dashed) and the Rh−$C_{(methyl)}$ distances. During the dissociation process which sets in at RCL = 1.6 Å (Figure 6B, full line sloping upward), the hydride atom H(1) stays weakly bonded to the Rh atom and provides a kind of intermediate monohapto bonding which lasts up to RCL = 1.4 Å, while the methyl group becomes mobile. The process can be visualized as the CH_3 group dissociating from the metal center and "dragging" the hydride behind. Comparison of the curves in Figure 6B with the equilibrium Rh−H(1) and Rh−$C_{(methyl)}$ distances (as indicated by thin horizontal lines) shows that the Rh−H(1) bond is strengthened initially, due to the net gain in electron density at the coordination center during the reductive elimination process. The lower coordination number and diminished hydride trans effect that result from CH_4 ejection can also be seen from the contraction of the Rh−$C_{(carbonyl)}$ distance in Figure 6C. Ejection is also followed by a rapid relaxation around the metallic center, which immediately returns to the square planar configuration after CH_4 has been removed, as shown by the increase of the Cl−Rh−CO angle (Figure 6D). The force on the RC, which is given in Figure 6E, shows that the transition state (zero of force) is reached at ~1.5 Å RCL, consistent with the structural data of Figure 6A−D. Once the CH_4 moiety is released, the force on the RC ceases to fluctuate since it is decoupled from the low-frequency vibrations around the metallic center.

Figure 6F shows the reaction enthalpy to be in the order of −120 kJ/mol and the activation energy to be about 70 kJ/mol, which is in good agreement with the ADF result of −115 and 72 kJ/mol.

The point charges for rhodium, hydride, and methyl carbon are shown in Figure 6G, analogously to Figure 5F. The curves show the behavior expected for reductive elimination. The process of charge transfer is continuous and does *not* take place abruptly on dissociation. Transfer of charge from the ligands to rhodium is gradual, which is related to the fact that the hydride atom is weakly associated with the Rh center although the Rh−C bond is already broken.

The time dependence of some key vibrational frequencies mirrors trends present in geometric parameters: The carbonyl stretching vibration changes abruptly from 1950 to 1850 cm^{-1} on CH_4 dissociation, indicating a weakening of the C−O bond caused by a strong contraction of the Rh−$C_{(carbonyl)}$ bond (Figure 6C), consistent with the change in the formal oxidation state of the Rh atom from +3 to +1. The Rh−hydride stretching frequency increases linearly from 2000 (RC = 2.6 Å, equilibrium geometry) to 2100 cm^{-1} (before dissociation at 1.4 Å RCL). It drops to 0 cm^{-1} at 1.4 Å RCL, since the ejection is a purely translational motion. The 100 cm^{-1} increase of the Rh−hydride stretch frequency is in line with our observed shortening of the Rh−hydride bond distance (Figure 6B). The Rh−$C_{(methyl)}$ stretch exhibits the same pattern, although with a smaller frequency change from 1250 cm^{-1} (2.6 Å) to 1300 cm^{-1} (1.4 Å) it drops at dissociation to 0 cm^{-1} at 1.4 Å RCL.

6. Conclusion

We have studied the electronic and molecular structures of $Rh(PH_3)_2(CO)Cl$ (**1**) and $Rh(PH_3)_2Cl$ (**2**) as models for respectively the precatalyst $Rh(PR_3)_2(CO)Cl$ and active species $Rh(PR_3)_2Cl$ involved in the catalytic alkane functionalization processes developed by Sakakura[4] and Tanaka (Figure 1). The square planar Vaska-type complex $Rh(PH_3)_2(CO)Cl$ (**1**) has a ground state conformation with the two phosphines in a trans position, *trans*-**1a**, whereas the cis isomer *cis*-**1a**, is 37 kJ/mol higher in energy. Complex **1** has two metal-to-ligand charge transfer transitions in the region 300−380 nm which lead to CO dissociation. The 14-electron species $Rh(PH_3)_2Cl$ (**2**) formed by photoejection of CO has a preferred cis conformation, *cis*-**2a**, with a closed-shell singlet ground state. The trans conformation *trans*-**2a** is 69 kJ/mol higher in energy. It is suggested that *trans*-**2a** initially is created by photolysis of *trans*-**1a**. The more stable isomer *cis*-**2a** is subsequently formed in an isomerization process with a calculated barrier of 41 kJ/mol via Y-shaped transition state **8**. The coordinatively unsaturated species *cis*-**2** was found to dimerize with a reaction enthalpy of −87 kJ/mol monomer. The dimerization process will reduce the catalytic activity of $Rh(PR_3)_2Cl$.

We have further studied the oxidative addition, **2** → **3** → **4** → **5**, and reductive elimination, **6** → **7** → **1**, of methane as model processes for important steps in alkane functionalization processes developed by Sakakura[4] and Tanaka, Figure 1. The oxidative addition of a C−H methane bond to the metal center in **2** is initialized by the formation of dihapto complex $Rh(PH_3)_2Cl(\eta^2\text{-}CH_4)$ (**3**) followed by transition state **4** in which the C−H bond is nearly broken (C−H = 1.5−1.6 Å). We have shown that though *trans*-**3** is very stable, it is also considerably mobile (high out-of-plane mobility of the CH_4 molecule) and thus prone to fast solvent exchange equilibria. Only an approach path inside the plane of *trans*-**2a** is energetically favorable. Weak, reversible η^1-bonding sets in at early stages of the reaction. Furthermore, evidence has been presented that the C−H activation product *trans*-**5a** is very likely to undergo fluxional processes subsequent to activation. The less stable *trans*-**2a** isomer forms a stronger dihapto complex and is more reactive toward the C−H bond than *cis*-**2a**. We have finally found that the reductive elimination from $CH_3(H)Rh(PH_3)_2(CO)Cl$ is relatively facile with kinetic barriers of 72 kJ/mol (trans) and 57 kJ/mol (cis), respectively. Dynamical simulations show that it occurs via a slow detachment of the methyl group, with subsequent dissociation of the hydride from the metal center and relaxation of *trans*-**1** into the square planar configuration. In addition, the elimination reactions are exothermic by respectively 112 kJ/mol (trans) and 125 kJ/mol (cis), Figure 4. Thus, the reductive elimination **6** → **7** → **1** will seriously retard alkane functionalization.

Acknowledgment. This work has been supported by the National Sciences and Engineering Research Council of Canada (NSERC), as well as by the donors of the Petroleum Research Fund, administered by the American Chemical Society (ACS-PRF No 20723-AC3). P.M. would like to thank the Austrian Fonds zur Förderung der wissenschaftlichen Forschung (FWF) for financial support within project JO1099-CHE.

JA952734V